Size dependence of the magnetic properties of antiferromagnetic Cr_2O_3 nanoparticles

D. Tobia, E. Winkler, R. D. Zysler, M. Granada, and H. E. Troiani
Centro Atómico Bariloche, CNEA-CONICET, 8400 San Carlos de Bariloche, Río Negro, Argentina
(Received 4 February 2008; revised manuscript received 6 August 2008; published 17 September 2008)

Magnetic properties of antiferromagnetic (AFM) Cr_2O_3 nanoparticles have been studied as a function of the nanoparticle size. The synthesized nanoparticles present an ellipsoidal shape with the major axis of approximately 170 nm and the minor axis that increases with the synthesis temperature from 30 to 70 nm. By magnetization and electron paramagnetic resonance experiments, we have obtained the parameters that characterize the AFM nanoparticles system. We have found that the Néel temperature, T_N, and the spin-flop field, H_{SF}, increase with the particle size from $T_N=288$ K and $H_{SF}(5\ \mathrm{K})=10$ kOe for the smaller nanoparticles and approach the bulk values [$T_N=308$ K and $H_{SF}(5\ \mathrm{K})=60$ kOe] for the larger particles. From the experimental results and the molecular-field theory applied to AFM coupled sublattices, we estimated the magnetic anisotropy, K, and the molecular-field constant, λ, as a function of the Cr_2O_3 nanoparticle size. When the size is reduced, λ only diminishes $\sim 8\%$ with respect to its bulk value (4.9×10^4 Oe^2 g/erg); instead, K decreases more than an order of magnitude from $K=3.8\times10^4$ to 8.7×10^2 erg/g. We analyzed the results on the basis of a core shell model where the nanoparticle internal order consists of an antiferromagnetically ordered core and a disordered surface shell, which presents a frustrated magnetic state.

DOI: 10.1103/PhysRevB.78.104412 PACS number(s): 75.50.Ee, 75.75.+a, 75.50.Tt, 76.30.−v

I. INTRODUCTION

The physical properties of a material are modified when their dimensions are reduced to the nanometric scale. This fact has impulsed the fabrication and study of nanosystems looking for new properties and applications.[1,2]

In magnetic nanoparticles, for example, when the diameter is reduced an increasing fraction of atoms lies at or near the surface and then surface and interface effects become more and more important. The presence of defects, broken exchange bonds, fluctuations in the number of atomic neighbors, and interatomic distances induce surface spin disorder and frustration. As a consequence the internal magnetic order and the magnetic phase transitions depend on the nanoparticles size.[3,4]

The surface disorder affects both the exchange and anisotropy fields and, as a consequence, the magnetic properties of a nanostructured material are different than those of the bulk. The ferromagnetic (FM) or ferrimagnetic nanoparticles present a huge magnetic moment that usually masks the size effects. For this reason the antiferromagnetic (AFM) materials are the suitable systems to study the surfaces and interfaces in nanoparticles.[5] In the AFM system the exchange field, H_E, that gives the antiparallel coupling between the magnetic sublattices is usually much stronger than the magnetic anisotropy field, H_A. However, H_A stabilizes the antiparallel spin order and plays a crucial role in the static and dynamic response of the system. In nanostructured materials with FM/AFM interfaces, it is well known that the antiferromagnetic anisotropy field is the crucial parameter that controls the exchange coupling through the interface.[6] Therefore, for the development and improvement of new applications based on the exchange bias phenomenon as ultra-high-density magnetic recording,[7] spin valves,[8] or the fabrication of new permanent magnetic materials,[9] it is fundamental to know the evolution of the anisotropy field with the size.

In the molecular-field approximation for two AFM coupled sublattices the exchange field is given by $H_E=\lambda M$, where λ is the molecular-field constant and M is the sublattice magnetization. In the case of uniaxial anisotropy, the anisotropy field is $H_A=K/M$, where K is the anisotropy constant.[10] When $H_A\neq0$, the response of the AFM system is very different if the magnetic field is applied along or perpendicular to the anisotropy axis. When an increasing magnetic field is applied perpendicular to the easy axis, the magnetic moments are reoriented until they line up with the applied magnetic field. Instead, if a growing magnetic field is applied along the easy axis, for small fields the magnetic sublattices remain along the symmetry axis, and then at a certain field value the sublattices suddenly reorient perpendicular to the symmetry axis maintaining the AFM array. This critical field is called spin-flop (SF) field, H_{SF}, and can be calculated from the difference between the free energy of the parallel and perpendicular configurations of the magnetic sublattices with respect to the easy axis. Therefore, $H_{SF}^2=2K/(\chi_\perp-\chi_\parallel)$, where $\chi_\perp$ and $\chi_\parallel$ are the perpendicular and parallel susceptibilities, respectively, and $\chi_\perp\sim1/\lambda$ when $H_E\gg H_A$. As can be seen, the SF transition provides information of the anisotropy and exchange fields, which in an AFM system is generally difficult to be obtained through other experiments.

Although it is well known that the magnetic properties are strongly affected by the surface to volume ratio, very few studies are reported on the influence of the size on the AFM and SF transitions.[11] Besides, as we mentioned previously, the surface disorder affects both the exchange and anisotropy fields. However, there are no systematic studies of the evolution of these parameters with the nanoparticle size; despite these fields determine the magnetic response of the system. With this motivation in mind we have synthesized Cr_2O_3 nanoparticles and have studied their magnetic properties as a function of the nanoparticle sizes by magnetization and electron-spin-resonance (ESR) experiments. This material

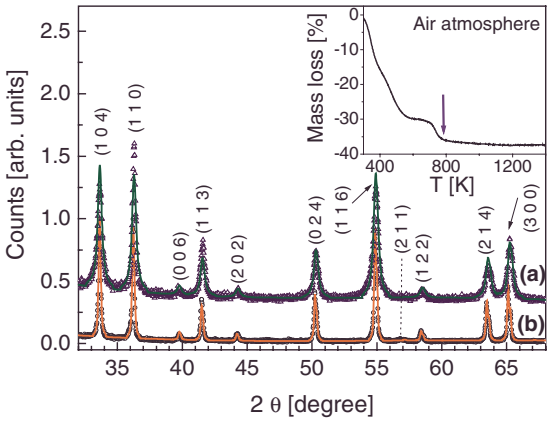

FIG. 1. (Color online) X-ray diffraction patterns (open symbols) of the Cr_2O_3 nanoparticles synthesized at (a) 873 and(b) 1673 K. The solids lines corresponds to the calculated profile. The (h k l) indices of the $R\bar{3}c$ phase are indicated. The inset shows the thermogravimetric (TGA) curve of the precursor measured in air atmosphere. Note that the Cr_2O_3 phase is fully formed above 730 K.

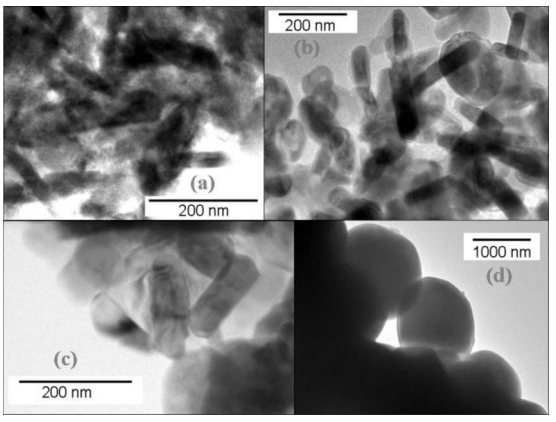

FIG. 2. TEM images of different samples annealed at (a) 1073, (b) 1573, and (c) 1673 K. Picture (d) shows the sample synthesized from chromium nitrate annealed at $T=1673$ K.

presents several advantages to perform this investigation, e.g., it has uniaxial crystal structure and two AFM sublattices spin order, which makes this compound a model system to study the spin-flop transition. The Cr_2O_3 crystallizes with the corundum structure ($R\bar{3}c$) presenting a unique threefold axis along the (111) direction. Below the Néel transition temperature ($T_N=308$ K), in zero magnetic field, the Cr^{3+} spins align antiferromagnetically along the (111) easy axis where the magnetic moments are alternated in an (+−+−) array for the *bacd* chromium sites in the corundum structure.[12,13] At the spin-flop transition the spins are reoriented in the basal plane maintaining the AFM order.[14,15] Due to the high T_N and the relatively low spin-flop field ($H_{SF}\sim 60$ kOe at low temperature in the bulk system), it is feasible to study this material at the temperature and field range used at the laboratory. Finally, as we have mentioned previously, this study gives us a unique possibility to calculate the anisotropy and exchange fields, which are difficult to obtain in an AFM material by other means.

II. SAMPLE PREPARATION AND CHARACTERIZATION

The Cr_2O_3 nanoparticles were synthesized from chromium hydroxide $Cr(OH)_3$ by chemical route.[16,17] The $Cr(OH)_3$ was prepared by mixing aqueous solutions of $CrK(SO_4)_2\cdot 12H_2O$ and KOH at pH ~ 10. The solution was kept in a reflux system for five days at approximately 380 K and then the product was dried in an oven at 340 K. Thermogravimetric measurements of the synthesis product performed in air atmosphere (inset of Fig. 1) show that the Cr_2O_3 phase is fully transformed at 730 K. Therefore in order to fabricate Cr_2O_3 nanoparticles of different sizes, the green powder was calcined in air atmosphere at different synthesis temperatures from 873 to 1673 K for 6 h. The x-ray diffraction patterns of the powder correspond to the $R\bar{3}c$ Cr_2O_3 phase for all the sample without any trace of other phases. Figure 1 shows the x-ray diffraction patterns corresponding to the samples annealed at 873 and 1673 K. From these measurements a clear broadening of the diffraction peaks and a shift toward higher angles can be observed for the lowest synthesis temperature. These results indicate that the particle size increases and the unit cell expands when the synthesis temperature increases. The nanoparticle size will be reported below from transmission electron microscopy (TEM) measurements, which allow us to obtain a more precise and complete information regarding the size distribution and particle shape. The evolution of the lattice parameters and the cell volume were calculated by means of the Rietveld method, using the FULLPROF refinement program.[18] We found that the a lattice parameter grows with the synthesis temperature and approaches the bulk value for the higher temperature. The lattice parameter a values for the samples annealed at 873, 1073, and 1673 K, are 4.9513(8), 4.9541(7), and 4.9588(4) Å, respectively, and the reported bulk value is $a=4.9587(1)$ Å (JPCDS-ICDD card 38–1479). Instead the c parameter remains almost unchanged in the studied samples, its value being $c=13.597(3)$ Å, similar to the bulk value [$c=13.5942(7)$ Å] within the error bar. The calculated cell volume grows from 288.68(9) to 289.40(5) Å^3 when the synthesis temperature increases. This expansion is related to the relaxation of the crystalline structure when the synthesis is performed at higher temperature.

The particle size distribution was determined from TEM images. The TEM measurements were performed in a Philips CM200 UT instrument operating at 200 kV. Figure 2 shows typical TEM images for some of the studied systems. These images show that the particles have ellipsoidal shape with a minor axis that increases with the synthesis temperature. However, the major axis keeps approximately a constant value of 170 nm. We have also prepared the bulk system by annealing the chromium nitrate $Cr(NO_3)_3\cdot 9H_2O$ at 1673 K for 24 h. TEM images of this sample show large round shaped particles with a mean diameter of 1500 nm [Fig. 2(d)]. Typical size distribution histograms obtained from the TEM micrographs are shown in Fig. 3, and Table I presents the average minor diameter for samples with different synthesis temperatures. Note that although the size distribution is broad the lattice parameter and the average nanoparticle

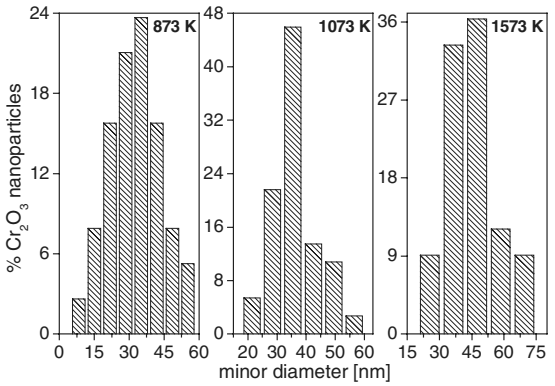

FIG. 3. Particle minor size diameter distribution measured from the TEM images for the samples synthesized at 873, 1073, and 1573 K.

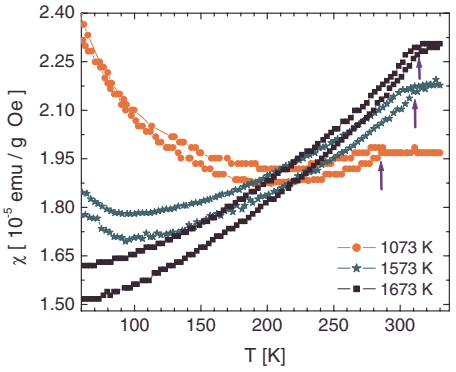

FIG. 4. (Color online) Temperature dependence of the susceptibility for Cr_2O_3 systems with different particle sizes measured applying a field $H=50$ Oe. Notably, T_N shifts to lower temperatures when the nanoparticles size decreases.

size follows a systematic behavior with the synthesis temperature.

The magnetic properties were investigated in the 5–350 K temperature range in applied fields up to 7 T by using a commercial superconducting quantum interference device (SQUID) magnetometer. The ESR spectra were recorded by a Bruker ESP300 spectrometer at 9.5 GHz for temperatures ranging from 100 K up to 500 K.

III. EXPERIMENTAL RESULTS AND DISCUSSION

A. Magnetization

Figure 4 shows the temperature dependence of the susceptibility for different samples where the AFM transition temperature T_N is pointed out by the arrows. From these curves it is evident that T_N shifts to lower temperatures when the nanoparticles size is reduced. We will return to this point later with the ESR results; this technique is more sensitive to the AFM transition so T_N is better determined. Note that for the largest nanoparticles the susceptibility presents the typical three-dimensional (3D)-AFM temperature dependence where the susceptibility monotonously decreases for $T<T_N$ and $\chi(T\rightarrow 0)\sim 2/3\chi_{\max}$. Instead, when the size is reduced the measurements show an increase in the susceptibility below T_N. This systematic increase in the susceptibility at low temperature was observed in several AFM nanoparticle systems and is attributed to the uncompensated spins located at the surface that present a frustrated AFM order.[19,20]

A typical field dependence of the magnetization is shown in Fig. 5 for the sample calcined at 1573 K. All the samples show a nonlinear behavior with an increase in the magnetization at high field, characteristic of the spin-flop transition. The low-field dependence of the magnetization at low temperature evidences a small irreversibility that goes to zero when the particle size increases. The upper inset of Fig. 5 shows the coercive field as a function of the synthesis temperature measured at $T=5$ K. The small magnetization irreversible component is mainly originated by the uncompensated surface spins and does not affect the spin-flop process, which develop in the AFM order core at higher fields. In all the studied cases the spin-flop transition develops in a broad field range. This fact is a consequence of a distribution of effective fields in the nanoparticle system due to the broad

TABLE I. Parameters obtained from TEM and ESR measurements for the different nanoparticles systems.

Synthesis T (K)	Minor diameter (nm)[a]	$T_N(K)$	β
873	30 (10)	288 ± 1	−0.7
1073	36 (6)	290 ± 1	−0.8
1273	50(10)	303 ± 1	−1.7
1573	47(10)	302 ± 1	−1.7
1673	70(10)	303 ± 1	−1.7
1673[b]	1500 (100)	304 ± 1	−1.7

[a]In parenthesis it includes the width at the half height of the size distribution obtained by TEM.
[b]Powder synthesized from chromium nitrate.

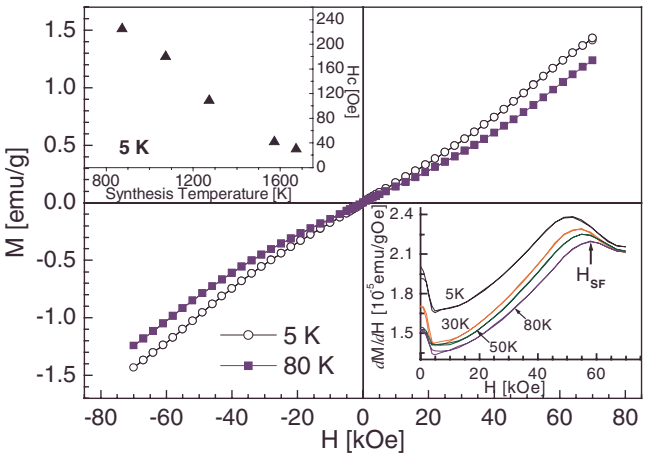

FIG. 5. (Color online) M vs H for the sample annealed at 1573 K for several temperatures. The spin-flop transition is indicated by the change in the curvature of the $M(H)$. Lower inset: numerical derivative of the M vs H curve for the sample annealed at 1573 K. Upper inset: Coercive field as a function of the synthesis temperature measured at $T=5$ K.

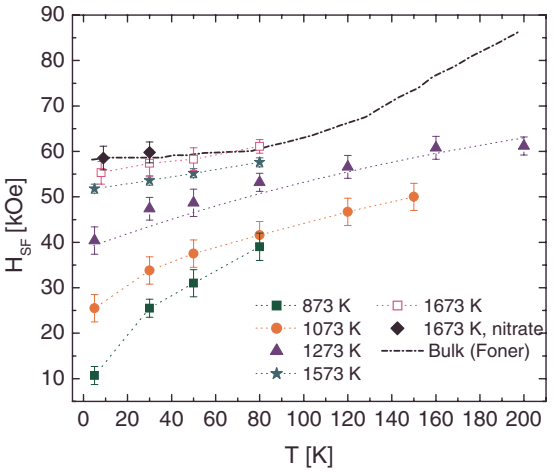

FIG. 6. (Color online) $H_{SF}(T)$ values for the samples synthesized at different temperatures. H_{SF} increases with the annealing temperature, i.e., with the particle size. The point-dash line corresponds to the H_{SF} values reported by Foner for a bulk sample (Ref. 14).

size distribution, as can be seen from the TEM histograms (Fig. 3). The nanoparticle powder system also presents an angular distribution of the anisotropy axis, which implies that only the particles with the easy axis oriented parallel to the external field (or close to this direction) develop a spin-flop transition. In order to determine the transition field we have performed the numerical derivative of the $M(H)$ curve. Following Ref. 11 we have defined H_{SF} as the maximum in the derivative curve as it is shown in the lower inset of Fig. 5.

The temperature dependence of H_{SF} for different nanoparticles sizes is plotted in Fig. 6. We have also included, for comparison, the H_{SF} (T) of the Cr_2O_3 bulk system reported by Foner in Ref. 14. These figures evidence a clear correspondence between the H_{SF} and the nanoparticles size, i.e., the transition field increases with the size and approaches to the bulk value for the larger nanoparticles. It is also worth remarking that in all the cases the spin-flop field follows the general temperature dependence predicted by the molecular-field approximation where H_{SF} increases when the temperature rises. This dependence is a characteristic for AFM systems because the difference $\chi_\perp - \chi_\parallel$ decreases faster than the magnetic anisotropy constant K when the temperature increases.[10] A precise description of the temperature evolution of the spin-flop field with the particle size (i.e., the temperature dependence of the anisotropy field for the different sizes) requires the measurement of $\chi_\perp(T)$ and $\chi_\parallel(T)$, which is very difficult to perform in a single nanoparticle. However, from the extrapolation of H_{SF} at $T=0$ (see Fig. 7) the size dependence of the anisotropy field can be calculated (as we are going to show in Sec. III C). This information allows us to know how sensitive is K to the disorder originated by the increase in the surface to volume ratio.

The size effect is also manifested in the temperature dependence of the high-field magnetization. Figure 8 shows $M(T, H=50$ kOe) where a clear increase in the magnetization is observed when the size is reduced. We want to remark that all the samples follow this monotonous increase in

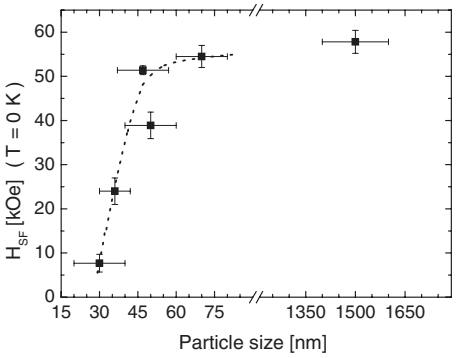

FIG. 7. H_{SF} extrapolated at $T=0$ K as a function of the minor diameter of the particle (the average minor diameter size has been taken from the center of the distribution measured by TEM, and the horizontal bars correspond to the width at the half height of the size distribution). Note that H_{SF} increases with the particle size and it saturates to the bulk value.

$M(T, H=50$ kOe) with size; however, from the spin-flop transition reported in Fig. 6 we can see that only the samples synthesized at 873, 1073, and 1273 K are in the SF phase at $H=50$ kOe. The larger nanoparticles have the transition to the spin-flop phase at higher magnetic fields. Therefore, in Fig. 8 we only compare the magnetization evolution of samples in the same magnetic phase. In an AFM system, the systematic increase in the magnetization at high fields and the increase in the irreversibility in the $M(H)$ curves (upper inset of Fig. 5) when the surface to volume ratio increases is coherent with an increasing fraction of uncompensated spins located at the surface when the size of the particles is reduced.

B. Electron paramagnetic resonance

In order to gain insight into the internal magnetic order of the Cr_2O_3 nanoparticles and the effective fields H_A and H_E, we have performed ESR experiments. This technique gives us complementary information to that obtained by the dc measurements and it is usually more sensitive to the magnetic transitions. In Fig. 9 we show the typical ESR spectra

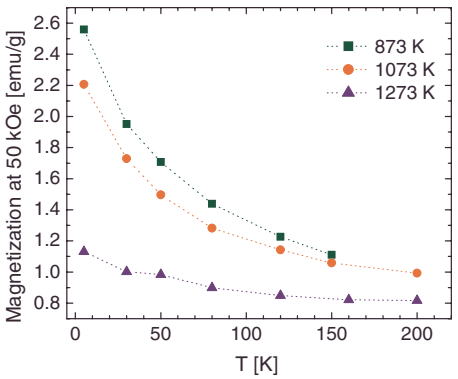

FIG. 8. (Color online) Magnetization measured at $H=50$ kOe for different samples as a function of temperature in the spin-flop phase where an increment of the magnetization when the particle size decreases is observed.

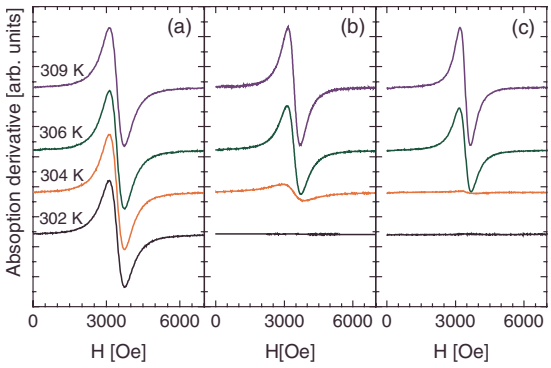

FIG. 9. (Color online) ESR spectra of the Cr_2O_3 system annealed at (a) 1073, (b) 1273, and (c) 1673 K (from nitrate) for several temperatures close to the AFM transition.

at several temperatures for the samples synthesized at 1073, 1273, and 1673 K (synthesized from nitrate). The high-temperature ESR spectra consist of a single absorption line centered at 3400 Oe, which disappears at the AFM order temperature. The size dependence of the transition temperature is remarkable, for the larger particles the spectra vanish at $T=304$ K, while for the smaller nanoparticles the resonance signal is still observed at $T=284$ K. From the ESR spectra we have obtained three experimental parameters: the resonance field (H_r), the linewidth (ΔH_{pp}), and the intensity (I). From the resonance field at $T>T_N$, we have achieved the gyromagnetic factor $g=1.977(2)$ for all the systems, which corresponds to the paramagnetic (PM) resonance of the Cr^{3+} ions ($3d^3$, $S=3/2$). The temperature dependence of the ESR I is shown in the inset of Fig. 10 where the intensity was calculated as $\Delta H_{pp}^2 \times h_{pp}$, where ΔH_{pp} is the peak to peak linewidth and h_{pp} is the peak to peak amplitude. As it is known, if all the magnetic ions contribute to the resonance, the ESR intensity is proportional to the susceptibility in the PM phase. Instead, below the AFM transition the microwave cannot reach the resonance condition due to the presence of large anisotropy and exchange fields, and as a consequence the ESR signal vanishes at T_N. Figure 10 shows the peak to peak linewidth $\Delta H_{pp}(T)$ for the different Cr_2O_3 nanoparticle

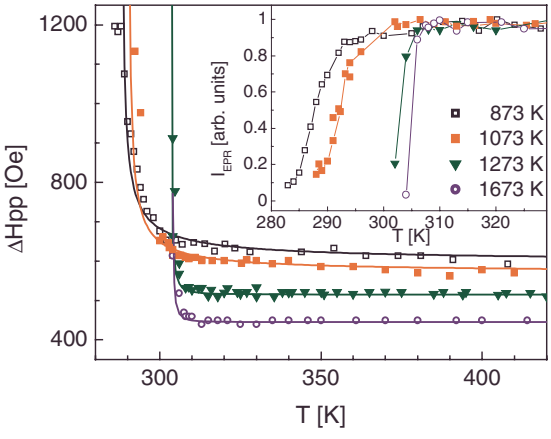

FIG. 10. (Color online) ΔH_{pp} vs T for different systems. The solid line corresponds to the linewidth calculated from Eq. (1). Inset: ESR intensity as function of temperature.

systems. In all the cases the linewidth is essentially temperature independent for $(T-T_N)>10$ K, while close to the transition temperature the linewidth increases up to twice its high-temperature value. Figure 10 clearly evidences the dependence of the order temperature with the particle size, i.e., T_N diminishes when the nanoparticle size is reduced.

It must be emphasized, that below T_N no paramagnetic signal was observed in the samples. This behavior contrasts with other studied nanoparticle systems, e.g., Mn_3O_4 nanoparticles[21] where the surface spins remain PM below the magnetic transition temperature. Consequently, in the Mn_3O_4 nanoparticle system the PM resonance signal of the surface spins is observed at low temperatures. Instead, in the present case, the vanishing of the ESR signal at T_N implies that all the spins in the nanoparticle are AFM correlated. This result complements the information obtained by the magnetization experiments, which evidences the presence of spins with magnetically frustrated order besides the main AFM state. Therefore the ESR and magnetization results are consistent with the core shell model proposed by Bhowmik *et al.*[19] for AFM nanoparticles. In this model the total magnetization of the particle is expressed as $M=\alpha M_{shell}\Sigma_{ij}\cos\theta_{ij}+(1-\alpha)M_{core}$, where θ_{ij} is the angle between the i and j spins and α is the shell thickness that increases when the particle size decreases. For the core spins, θ_{ij} is 180°, while the angle between adjacent shell spins could have any value between $0<\theta_{ij}<180°$. When α increases, more shell spins apart from their antiparallel alignment. As a consequence, the system is modeled as an antiferromagnetically ordered core with a shell where the spins are in a magnetically frustrated array and the shell/core ratio increases when the particle size decreases.

In order to obtain the average transition temperature as a function of the nanoparticle size, we have analyzed and simulated the experimental results in the PM regime near the magnetic critical point. In a polycrystalline sample the temperature dependence of the ESR linewidth above the order transition temperature is given by[22–24]

$$\Delta H_{pp}(T) = \left\{ \frac{C}{T\chi(T)} \Delta H_\infty \right\} \{1 + A(T - T_m)^\beta\}. \qquad (1)$$

The first and second terms of Eq. (1) correspond to the noncritical and critical contribution to the linewidth, respectively, ΔH_∞ is the high-T value for $\Delta H_{pp}(T)$, C is the Curie constant, T_m is the transition temperature, and β is the critical exponent. In the AFM system the susceptibility varies slowly near T_N so the temperature dependence of the linewidth is mainly described by the second term of Eq. (1). Therefore in many systems the first term can be approximated by a constant value equal to the high-temperature linewidth, as for example in the uniaxial antiferromagnet MnF_2 (Ref. 25) and the spinel $ZnCr_2O_4$.[26] Near the AFM transition, theoretical studies of the $\Delta H_{pp}(T)$ for AFM systems predict a critical exponent value of $\beta=-5/3$ (Refs. 27 and 28); however none theoretical study includes finite-size effects. From Eq. (1) and approximating the first term by the high-temperature linewidth value, we have simulated $\Delta H_{pp}(T)$. The simulated curves are shown in Fig. 10 (solid lines) and the obtained transition temperatures and critical exponent

values are presented in Table I. Note that T_N remains almost unchanged in the samples synthesized at higher temperatures. Instead, in the nanoparticles synthesized at lower temperatures the finite-size effects begin to affect the magnetic order and as a consequence T_N shifts toward lower temperatures. From Fig. 10, it can also be noticed that in the case of the larger particles there is a good agreement between the experimental linewidth and the one simulated with the theoretical critical exponent. Instead, when the size diminishes the transition broadens as a consequence of finite-size effects, size dispersion, and the surface disorder. This behavior is reflected in a large distribution of transition temperatures and a decrease in the magnitude of the critical exponent. The contributions of these two factors to the transition broadening cannot be distinguished from our experiment. Very few studies are reported in the literature about the ESR parameters of nanoparticles near the transition temperature. The ESR studies of Refs. 29 and 30, performed on Co_3O_4 AFM nanoparticles, point out that the critical term is more important in the samples with smaller particle size so that short-range magnetic order above T_N is detected over a wider temperature range. This result is in agreement with the broadening of the transition observed in our measurements when the particle size diminishes. However, the evolution of the critical parameter is not reported. ESR experimental studies near the transition temperature (in particular at lower excitation frequency so that the magnetic field does not broaden the transition) and a theory of the relaxation rate for spin fluctuation in nanostructures are necessary to have a complete understanding of the spin dynamics of the nanoparticle system.

C. Exchange and anisotropy

In the above sections we have presented the evolution of the Néel temperature and the spin-flop field for the different particles systems by ESR and magnetization experiments. For the larger particles both parameters remain almost unchanged, and below ~50 nm T_N and H_{SF} present a clear departure of their bulk behavior. It is notable that while T_N only diminishes 20 K from the bulk value, H_{SF} decreases from 60 to 10 kOe for the smallest nanoparticles. From T_N and the results of molecular-field theory for two AFM coupled sublattices, we can calculate the effective exchange field as $|\lambda|=3k_B\ T_N/n\mu_{\text{eff}}^2$,[10] where n corresponds to the spin density, μ_{eff} is the effective magnetic moment, and k_B is the Boltzmann constant. We have applied this result to the Cr_2O_3 compound where each magnetic sublattice contains $1/2\ N\ Cr^{3+}$ ions with $S=3/2$, with N being the Avogadro constant. The calculated effective exchange constant for the different synthesis temperatures is shown in Fig. 11(a). Notice that λ follows the same behavior than the Néel temperature, it remains almost unchanged for the larger particles and decreases when the surface to volume ratio grows up. In the studied systems the exchange field constant only diminishes to 4.7×10^4 Oe^2 g/erg from the bulk value 4.9×10^4 Oe^2 g/erg when the size is reduced.

As we have mentioned in the introduction, the study of the spin-flop transition provides a way to calculate the anisotropy constant of the AFM system. Defining $\alpha=\chi_{\parallel}/\chi_{\perp}$, the spin-flop field is expressed as $H_{SF}^2=2\lambda K/(1-\alpha)$, and from this expression it is obtained as

$$H_{SF}^2(T\rightarrow 0)=2\lambda K. \tag{2}$$

From Eq. (2) and the exchange constant calculated from the ESR experiments we have determined the anisotropy constant K for the different particle sizes. Figure 11(b) displays the anisotropy constant as a function of the synthesis temperature where a systematic increase with the particle size is observed. The value of K for the larger particles approaches the one reported in Ref. 14 ($K=3.8\times10^4$ erg/g) for the Cr_2O_3 bulk single crystal.

We have found that the molecular-field constant is not very sensitive to the increase in the surface to volume ratio. As we have remarked, λ only diminishes approximately 8% from its bulk value; instead, the magnetic anisotropy constant decreases more than an order of magnitude (from $K=3.8\times10^4$ to 8.7×10^2 erg/g) when size is reduced. These results are in agreement with the fact that λ originated mainly from the nearest-neighbor interaction, while the magnetic anisotropy field is originated from dipolar and crystalline field contribution.[14] These last contributions depend on the crystalline array and therefore are strongly influenced by the disorder induced in the surface and the size effects at nanometric scale.

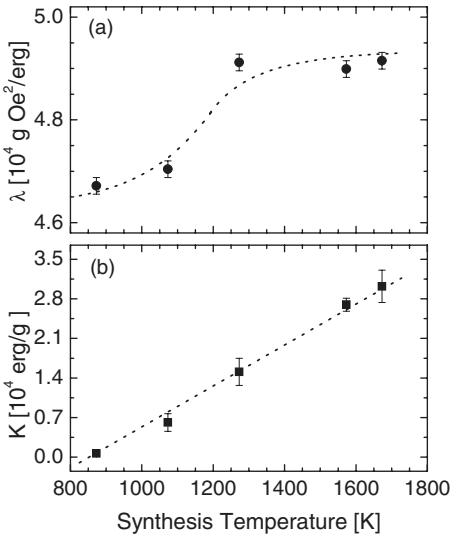

FIG. 11. (a) Molecular field constant (λ) of Cr_2O_3 and (b) anisotropy constant (K) as a function of the synthesis temperature (and therefore of the nanoparticle size). The dashed lines are a guide to the eyes. The λ value only diminishes ~8% with respect to its bulk value (4.9×10^4 Oe^2 g/erg), while K decreases more than an order of magnitude.

IV. CONCLUSION

We have studied the temperature and size dependence of the magnetic properties of antiferromagnetic Cr_2O_3 ellipsoidal nanoparticles. We have shown how the ESR measurements give fundamental information, which complements that obtained from magnetization measurements, and enable

us to calculate the characteristic parameters of the antiferromagnetic nanoparticles system. The results show that the surface disorder and spin canting increase when the particle size is reduced. This disorder yields to a weakening of the exchange interactions between the ions located near the surface and as a consequence the order temperature diminishes. The spin-flop transition presents a strong dependence with the particles size at nanometric scale. Finally, we have determined the anisotropy field, which presents a remarkable monotonous decrease when the nanoparticle size is reduced. This analysis can be easily extrapolated to other nanostructures where the knowledge of the AFM anisotropy is fundamental for the understanding of the basic properties and comprehension for the development of any specific device.

ACKNOWLEDGMENTS

The authors thank M. T. Causa for the valuable suggestions and discussions. This work was accomplished with partial support of ANPCyT Argentina through Grants No. PICTs 3–13294, No. 4–25317, and No. 20770, Conicet Argentina through Grant No. PIP 5250/03, and U. N. Cuyo through Grant No. 06/C275.

[1] J. L. Dormann, D. Fiorani, and E. Tronc, Adv. Chem. Phys. **98**, 283 (1997).
[2] *Magnetic Storage Systems Beyond 2000*, edited by G. C. Hadjipanayis (Kluwer, Dordrecht, 2001).
[3] X. Y. Lang, W. T. Zheng, and Q. Jiang, Phys. Rev. B **73**, 224444 (2006).
[4] X. G. Zheng, C. N. Xu, K. Nishikubo, K. Nishiyama, W. Higemoto, W. J. Moon, E. Tanaka, and E. S. Otabe, Phys. Rev. B **72**, 014464 (2005).
[5] S. Mørup, D. E. Madsen, C. Frandsen, C. R. H. Bahl, and M. F. Hansen, J. Phys.: Condens. Matter **19**, 213202 (2007).
[6] J. Nogués, J. Sort, V. Langlais, V. Skumryev, S. Suriñach, J. S. Muñoz, and M. D. Baró, Phys. Rep. **422**, 65 (2005).
[7] V. Skumryev, S. Stoyanov, Y. Zhang, G. Hadjipanayis, D. Givord, and J. Nogués, Nature (London) **423**, 850 (2003).
[8] J. C. S. Kools, IEEE Trans. Magn. **32**, 3165 (1996).
[9] J. Sort, J. Nogués, S. Suriñach, J. S. Muñoz, M. D. Baró, E. Chappel, F. Dupont, and G. Chouteau, Appl. Phys. Lett. **79**, 1142 (2001).
[10] A. H. Morrish, *The Physical Principles of Magnetism* (IEEE, New York, 2001).
[11] R. D. Zysler, D. Fiorani, A. M. Testa, L. Suber, E. Agostinelli, and M. Godinho, Phys. Rev. B **68**, 212408 (2003).
[12] C. G. Shull, W. A. Strauser, and E. O. Wollan, Phys. Rev. **83**, 333 (1951).
[13] J. O. Artman, J. C. Murphy, and S. Foner, Phys. Rev. **138**, A912 (1965).
[14] S. Foner, Phys. Rev. **130**, 183 (1963).
[15] M. Fiebig, D. Fröhlich, and H.-J. Thiele, Phys. Rev. B **54**, R12681 (1996).
[16] M. Bañobre-López, C. Vázquez-Vázquez, J. Rivas, and M. A. López-Quintela, Nanotechnology **14**, 318 (2003).
[17] S. A. Makhlouf, J. Magn. Magn. Mater. **272-276**, 1530 (2004).
[18] J. Rodríguez-Caravajal, Physica B **192**, 55 (1993).
[19] R. N. Bhowmik, R. Nagarajan, and R. Ranganathan, Phys. Rev. B **69**, 054430 (2004).
[20] A. Punnoose, H. Magnone, M. S. Seehra, and J. Bonevich, Phys. Rev. B **64**, 174420 (2001).
[21] E. Winkler, R. D. Zysler, and D. Fiorani, Phys. Rev. B **70**, 174406 (2004).
[22] D. L. Huber and M. S. Seehra, J. Phys. Chem. Solids **36**, 723 (1975).
[23] D. L. Huber, G. Alejandro, A. Caneiro, M. T. Causa, F. Prado, M. Tovar, and S. B. Oseroff, Phys. Rev. B **60**, 12155 (1999).
[24] M. T. Causa, M. Tovar, A. Caneiro, F. Prado, G. Ibáñez, C. A. Ramos, A. Butera, B. Alascio, X. Obradors, S. Piñol, F. Rivadulla, C. Vázquez-Vázquez, A. López-Quintela, J. Rivas, Y. Tokura, and S. B. Oseroff, Phys. Rev. B **58**, 3233 (1998).
[25] M. S. Seehra and T. G. Castner, Jr., Solid State Commun. **8**, 787 (1970).
[26] H. Martinho, N. O. Moreno, J. A. Sanjurjo, C. Rettori, A. J. García-Adeva, D. L. Huber, S. B. Oseroff, W. Ratcliff, S.-W. Cheong, P. G. Pagliuso, J. L. Sarrao, and G. B. Martins, Phys. Rev. B **64**, 024408 (2001).
[27] M. S. Seehra and D. L. Huber, AIP Conf. Proc. **24**, 261 (1975).
[28] D. L. Huber, Phys. Rev. B **6**, 3180 (1972).
[29] P. Dutta, M. S. Seehra, S. Thota, and J. Kumar, J. Phys.: Condens. Matter **20**, 015218 (2008).
[30] S. Angelov, E. Zhecheva, R. Stoyanova, and M. Atanasov, J. Phys. Chem. Solids **51**, 1157 (1990).